An Explicit Finite Volume Element Method without an Explicit Artificial Diffusion Term for Convection-Diffusion Equation on Triangular Grids

Sutthisak Phongthanapanich
Department of Mechanical Engineering Technology, College of Industrial Technology, King Mongkut's University of Technology North Bangkok, Bangkok 10800, Thailand
E-mail: sutthisakp@kmutnb.ac.th

Abstract

A high-resolution finite volume method for solving two-dimensional convection-diffusion equation on triangular meshes is presented. The concept of the finite element technique is applied to estimate the gradient quantities at the cell faces. It is shown that the method does not require any artificial diffusion to improve the solution stability. The robustness and accuracy of the method have been evaluated by using available analytical and numerical solutions of two-dimensional pure-convection and convection-diffusion problems.

Keywords: Convection-Diffusion Equation; Finite Volume Element Method; Explicit Scheme

1. Introduction

Computation of the transport phenomena in fluid dynamics is one of the most fundamental and difficult problems that arises in numerical simulation of the convection-diffusion equations. To be able to use available computational resources at an acceptable accuracy for practical applications, larger mesh size and time step are normally employed. Most of the current methods, however, suffer from serious numerical difficulties when the transport phenomenon is governed by a convection-dominated process. The oscillation of numerical solution with undershooting and/or overshooting may appear in the vicinity of steep gradient [1-4]. It is well-known that first-order schemes smear discontinuities over many cells resulting in low numerical reliability for long time computation. To overcome these problems, many higher-order numerical schemes have been introduced [5] to solve conservation law problems. Although the higher-order numerical schemes such as Lax-Wendroff, Beam-Warming, and Fromm schemes can reduce the smearing of discontinuities, the undershooting/overshooting still occur in the vicinity of discontinuities. This is because these higher-order numerical schemes are not monotone. The linear monotonicity-preserving schemes based on Godunov's theorem [6] are at most first-order accurate and yield poor stability conditions. To overcome the above problems, many non-linear methods such as the Total Variation Diminishing (TVD) [7], the Total Variation Bounded (TVB) [8], the

Range Diminishing [9], and the Normalized Variable Approach (NVA) [9] have been introduced. The development of an accurate numerical model for the convection-diffusion equations is still a challenging task in computational fluid dynamics [2,4,10-16].

There are many ways to discretize a given domain into small discrete triangular control volumes for finite volume computation [11]. In general, the classification depends on the choice of the control volumes and the discrete space to which the approximated solution belongs. In the overlapping control volume cell-vertex scheme, the flow variables are defined at the nodes while the control volumes coincide with triangles [17,18]. To relate the cell-based to the node-based residuals, an approximation is done by using the residual distribution formula. In the dual control volume cell-vertex scheme, the flow variables are defined at the nodes and the control volumes are centered around the nodes [19,20]. One popular scheme is to join the cell centroids to the edge midpoints of the neighboring cells. It should be noted that these cell-vertex schemes encounter difficulty on the treatment of boundary conditions to ensure a consistent solution at boundary points. In this paper, the cell-centered scheme is used such that the flow variables are defined at the cell centroids, and the control volumes coincide with triangles [11,21,22]. The treatment of boundary conditions is simple and straightforward because the control volumes are coincided with triangles.

To solve flow problems in practical applications, stable and accurate numerical schemes are necessary. Several higher-order schemes have been proposed and studied by many researchers [2,11-13,15,22,23,]. However, the drawback of the higher-order schemes is their non-monotonic solutions. Godunov [6] showed that higher-order schemes with constant coefficients are non-monotonic with oscillations appearing in the computed profiles. One possible way to suppress the oscillations is to apply a limiter function such that the monotony of the solution is preserved [7,24]. In this research work, the higher-order solution is approximated by determining the numerical flux along the cell face at the half time step by $f = f(\phi_{ij}^{n+1/2})$ [25-27]. The control volume reconstruction approach of $\phi_{ij}^{n+1/2}$ is performed by adopting the method of [22,28] through the expansion of ϕ_i with a Taylor's series expansion. The temporal term is estimated by adapting the idea of local expansion of unknown along the characteristics [2,29].

An explicit high-resolution finite volume method based on the second-order approximation is thus proposed in this paper for solving the two-dimensional convection-diffusion equation on triangular meshes. The robustness and accuracy of the proposed method have been examined by using the convection-dominated problems. For such problems as mentioned above, several schemes become unstable and produce node to node fluctuation [2]. To suppress the fluctuation, an artificial diffusion is normally added into the scheme [4]. One of the main objectives of the proposed method is to achieve the numerical stability without adding such artificial diffusion. This is to avoid excessive deterioration of the computed solution as it proceeds in time. The presentation of the paper starts from the explanation of the theoretical formulation in Section 2. The performance of the proposed method is then evaluated in Section 3 by using three examples.

2. Finite Volume Element Formulation

The governing differential equation for the two-dimensional convection-diffusion equation is:

$$\frac{\partial \phi}{\partial t} + \nabla \cdot (\boldsymbol{v}\phi - \varepsilon \nabla \phi) = 0 \quad (1)$$

subject to the boundary conditions

$$\phi = g_D \qquad \text{on } \partial\Omega_D \quad (2)$$

$$\varepsilon \frac{\partial \phi}{\partial n} = g_N \quad \text{on } \partial\Omega_N \quad (3)$$

where $\partial\Omega = \partial\Omega_D \cup \partial\Omega_N$ with $\partial\Omega_D \cap \partial\Omega_N = 0$ The variable ϕ is the unknown scalar quantity, $\boldsymbol{v} = \boldsymbol{v}(\boldsymbol{x})$ is the given convection velocity field, $\varepsilon \geq 0$ is the diffusion coefficient, and $t \in (0,T)$ with $T > 0$.

The initial condition is defined for $\boldsymbol{x} \in \Omega$ and $\Omega \subset R^2$ by $\phi(\boldsymbol{x},0) = \phi_0(\boldsymbol{x})$.

$$\phi(\boldsymbol{x},0) = \phi_0(\boldsymbol{x}) \quad (4)$$

The computational domain is first discretized into a collection of non-overlapping triangular control volumes $\Omega_i \in \Omega$, i=1,…, N, that completely cover the domain such that :

$$\Omega = \cup_{i=1}^{N} \Omega_i \,,\ \Omega_i \neq 0 \quad (5)$$

A higher-order numerical scheme can be obtained by integrating equation (1) over the control volume Ω_i and in the time interval (t^n, t^{n+1}) to obtain :

$$\int_{\Omega_i} \int_{t^n}^{t^{n+1}} \left(\frac{\partial \phi}{\partial t} + \nabla \cdot (\boldsymbol{v}\phi - \varepsilon \nabla \phi) \right) dt d\boldsymbol{x} = 0 \quad (6)$$

A temporal integration is applied to the first term, to yield:

$$\int_{\Omega_i} \phi(\boldsymbol{x}, t^{n+1}) d\boldsymbol{x} = \int_{\Omega_i} \phi(\boldsymbol{x}, t^n) d\boldsymbol{x} - \int_{\Omega_i} \int_{t^n}^{t^{n+1}} \nabla \cdot (\boldsymbol{v}\phi - \varepsilon \nabla \phi) dt d\boldsymbol{x} \quad (7)$$

In the conventional finite volume method, the approximation to the cell average of ϕ over Ω_i at time t^n and t^{n+1} is represented by [13,23]:

$$\phi_i^n = \frac{1}{|\Omega_i|} \int_{\Omega_i} \phi(\boldsymbol{x}, t^n) d\boldsymbol{x} \quad (8a)$$

$$\phi_i^{n+1} = \frac{1}{|\Omega_i|} \int_{\Omega_i} \phi(\boldsymbol{x}, t^{n+1}) d\boldsymbol{x} \quad (8b)$$

where $|\Omega_i|$ is the measure of Ω_i . The time integration of the flux terms on the right-hand side of equation (7) can be determined by many ways [25-27]. For the proposed scheme, the idea implemented by WAF scheme [30] is used to approximate the time integration by assuming that the time step is small enough for linear approximation and then applying the mid-point quadrature rule in time. The divergence theorem is then applied to yield:

$$\begin{aligned} &\int_{\Omega_i} \int_{t^n}^{t^{n+1}} \nabla \cdot (\boldsymbol{v}\phi - \varepsilon \nabla \phi) dt d\boldsymbol{x} \\ &= \Delta t \int_{\Omega_i} \nabla \cdot (\boldsymbol{v}\phi(\boldsymbol{x}, t^{n+1/2}) - \varepsilon \nabla \phi(\boldsymbol{x}, t^{n+1/2})) d\boldsymbol{x} \\ &= \Delta t \int_{\Omega_i} \boldsymbol{n}_i(\nu) \cdot (\boldsymbol{v}(\nu)\phi(\boldsymbol{x}, t^{n+1/2}) - \varepsilon \nabla \phi(\boldsymbol{x}, t^{n+1/2})) d\boldsymbol{x} \end{aligned} \quad (9)$$

where $\boldsymbol{n}_i(\nu)$ is the unit normal vector of $\partial\Omega_i$. For a triangular finite volume mesh, the flux integral over $\partial\Omega_i$ appearing on the right-hand side of equation (9) can be approximated by the summation of fluxes passing through the three adjacent cell faces. Then equation (9) can be approximated by:

$$\begin{aligned} &\int_{\Omega_i} \int_{t^n}^{t^{n+1}} \nabla \cdot (\boldsymbol{v}\phi - \varepsilon \nabla \phi) dt d\boldsymbol{x} \\ &= \Delta t \sum_{j=1}^{3} |\Gamma_{ij}| \boldsymbol{n}_{ij} \cdot (\boldsymbol{v}_{ij} \phi_{ij}^{n+1/2} - \varepsilon \nabla \phi_{ij}^{n+1/2}) \end{aligned} \quad (10)$$

where $\nabla\phi_{ij}^{n+1/2} = \nabla\phi_{ij}(t^{n+1/2})$, Γ_{ij} is the segment of boundary $\partial\Omega_i$ between two adjacent control volumes Ω_i and Ω_j, which are defined by:

$$\partial\Omega_i = \cup_{j=1}^{3}\Gamma_{ij} \tag{11a}$$

$$\Gamma_{ij} = \partial\Omega_i \cap \partial\Omega_j \tag{11b}$$

To arrive at an explicit scheme, $\nabla\phi_{ij}^{n+1/2}$ is approximated by $\nabla\phi_{ij}^{n}$. Such approximation is employed in the explicit CBS scheme [29,31]. Hence, equation (10) becomes:

$$\int_{\Omega_i}\int_{t^n}^{t^{n+1}} \nabla\cdot(\boldsymbol{v}\phi - \varepsilon\nabla\phi)dtd\boldsymbol{x} = \Delta t\sum_{j=1}^{3}\left|\Gamma_{ij}\right|\boldsymbol{n}_{ij}\cdot(\boldsymbol{v}_{ij}\phi_{ij}^{n+1/2} - \varepsilon\nabla\phi_{ij}^{n}) \tag{12}$$

By substituting equations (8) and (12) into equation (7) and dividing by $\left|\Omega_i\right|$, an explicit finite volume scheme for solving equation (1) is obtained in the form:

$$\phi_i^{n+1} = \phi_i^n - \frac{\Delta t}{\left|\Omega_i\right|}\sum_{j=1}^{3}\left|\Gamma_{ij}\right|\boldsymbol{n}_{ij}\cdot\left(\boldsymbol{v}_{ij}\phi_{ij}^{n+1/2} - \varepsilon\nabla\phi_{ij}^{n}\right) \tag{13}$$

The gradient term, $\nabla\phi_{ij}^{n}$, is determined by the weighted residuals method which is commonly used in the finite element technique [31]. Firstly, this $\nabla\phi_{ij}^{n}$ is assumed to distribute linearly over Ω_i in the form:

$$\nabla\phi_i^n = \sum_{j=1}^{3} N_j(\boldsymbol{x})\nabla\phi_j^n \tag{14}$$

where $N_j(\boldsymbol{x})$ denotes the linear interpolation functions for the adjacent control volumes. By applying the weighted residuals method and the Gauss's theorem to Eq. (14), the gradient quantities at the grid point are obtained as:

$$\nabla\phi_{j,i}^n = \boldsymbol{M}^{-1}\left(\int_{\partial\Omega_i}\boldsymbol{n}_i(\nu)N_j(\nu)\phi_i^n d\nu - \int_{\Omega_i}\frac{\partial N_j(\nu)}{\partial\boldsymbol{x}}\phi_i^n d\boldsymbol{x}\right) \tag{15}$$

where $\boldsymbol{M}$ is the consistent mass matrix [31], and $\nabla\phi_{j,i}^n$ are the contribution of gradient quantities in the finite volume mesh Ω_i to the gradient quantities at node *j*. As an example, Figure 1 shows five triangular finite volumes surrounding node *j*. In order to compute the total gradient quantities at node *j*, equation (15) is applied to all triangular finite volumes surrounding the node *j* such that:

$$\nabla\phi_j^n = \sum_{i=1}^{I}\nabla\phi_{j,i}^n \tag{16}$$

where *I* is the number of the surrounding triangular finite volumes. The nodal gradient recovery procedure above provides linear distribution profile and continuous across cell faces, the gradient quantities at Γ_{ij}, $\nabla\phi_{ij}^n$, is then computed by applying the mid-point quadrature rule along the edge connected to nodes *i* and *j*.

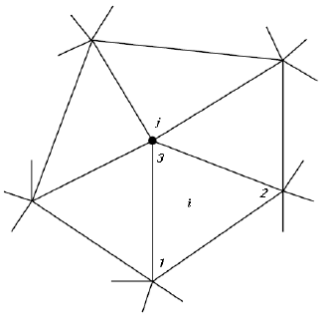

Figure 1 Triangular finite volumes surrounding node *j*.

Finally, the scalar quantities at the half time step $t^{n+1/2}$, $\phi_{ij}^{n+1/2}$, is approxi-

mated by applying the Taylor's series expansion in both space and time. The temporal derivative term may be estimated by adapting the idea of local expansion of unknown along the characteristics [2,29]. By assuming that the velocity is pointed in the direction from Ω_i to Ω_j, the value of $\phi_{ij}^{n+1/2}$ can be written in the form:

$$\phi_{ij}^{n+1/2} = \phi_i^n + \left(\boldsymbol{x}_{ij} - \boldsymbol{x}_i\right)\cdot\nabla\phi_i^n - \frac{\Delta t}{2}\left(\boldsymbol{v}_i\cdot\nabla\phi_i^n\right) \tag{17}$$

where $\boldsymbol{x}_i$ and $\boldsymbol{x}_{ij}$ are cell centroid and face centroid locations, respectively. For the first order scheme:

$$\phi_{ij}^{n+1/2} = \phi_i^n \tag{18}$$

For the opposite direction of velocity, the value $\phi_{ij}^{n+1/2}$ can be computed from equations (16) or (17) but using the values from the neighboring triangles according to the upwinding direction.

It is well-known that, to ensure the stability of the numerical scheme on triangular mesh, the CFL-like stability criterion must be fulfilled. In this paper, the time-step within each finite volume mesh is determined from:

$$\Delta t = C\min_i\left(\frac{|\Omega_i|}{\max\limits_{j=1,2,3}|v_{n,ij}|}, \frac{|\Gamma_i^c|^2}{2\varepsilon}\right) \tag{19}$$

where $v_{n,ij}$ is the scaled normal velocity at Γ_{ij}, $|\Gamma_i^c|$ is a cell characteristic length and $0 < C \le 1$. For the examples presented in this paper, the value of *C* is given as 1.0 for all pure-convection problems, and 0.5 for all convection-diffusion problems.

3. Numerical examples

To evaluate the robustness and accuracy of the proposed high-resolution finite volume method, both pure-convection and convection-dominated diffusion examples are examined. All examples presented in this section are tested using structured triangular meshes. These examples are: (1) the mixing of a hot front with a cold front, (2) the rotation of Gaussian pulse, and (3) the half-sine inflow convection-diffusion problems.

3.1 Mixing of a Hot Front with a Cold Front

The first example is a pure-convection problem for the mixing of a hot front with a cold front. The problem is examined on the domain $\Omega = [-4,4]^2$. The initial condition $\phi(\boldsymbol{x},0)$ is given by [11,14]:

$$\phi(\boldsymbol{x},0) = -\tanh\left(\frac{y}{2}\right) \tag{20}$$

The velocity field is given by:

$$u(\boldsymbol{x}) = -\frac{y}{r}\frac{f_t}{0.385} \tag{21a}$$

$$v(\boldsymbol{x}) = \frac{x}{r}\frac{f_t}{0.385} \tag{21b}$$

where *r* is the distance from the origin of the coordinate system, and the value of the function f_t is defined by:

$$f_t = \frac{\tanh(r)}{\cosh^2(r)} \tag{22}$$

This problem is examined until the final time *t*=4, for which the exact solution is given by:

$$\phi(\boldsymbol{x},4) = -\tanh\left(\frac{y}{2}\cos(\frac{4f_t}{0.385r}) - \frac{x}{2}\sin(\frac{4f_t}{0.385r})\right) \quad (23)$$

A uniform triangular mesh S1, 32 × 32 ($\Delta x = \Delta y = 1/32$) as shown in Figure 2 is used. Figures 3(a)-(d) show the exact solution at the final time t=4, and the corresponding numerical solutions from the three uniform meshes S1, S2, and S3 (32 × 32, 64 × 64, and 128 × 128), respectively. Even though this test case is performed without any flux-limiter function, the figures show that the numerical oscillation decreases as the meshes are refined (S2 and S3). To study the experimental order of convergence (EOC) of the proposed numerical scheme, the finer mesh S4 (256 × 256), and S5 (512 × 512) are tested. The comparison of exact and numerical solutions is shown in Figure 4(a), and the L_2-norm errors versus mesh sizes is shown in Figure 4(b). The L_2-norm error is computed from:

$$\|L_2\| = \left(\frac{1}{NP}\sum_{i=1}^{NP}(\phi_{i,exact} - \phi_i)^2\right)^{1/2} \quad (24)$$

where NP is number of nodes. The L_2-norm errors and computational times obtained from various mesh sizes are presented in Table 1. Figures 4(a)-(b) show that the computed solution converges to the exact solution as the mesh is refined. Finally, it is noted that the EOC value for this example is about two, as shown in Table 1.

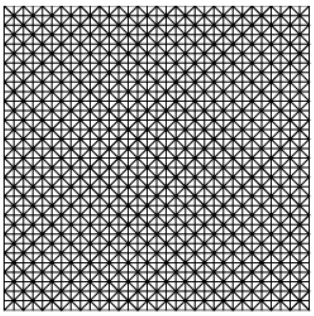

Figure 2 Uniform triangular grid S1.

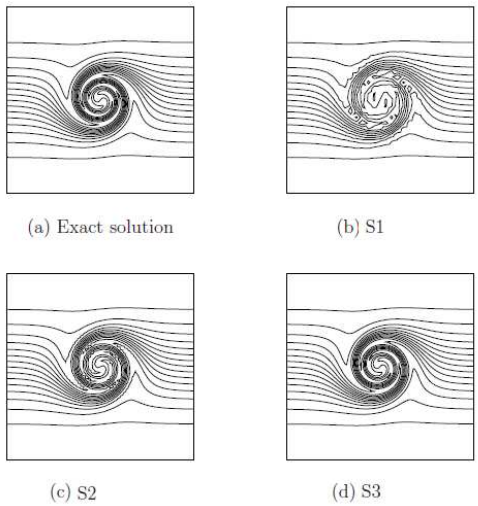

Figure 3 Comparison of exact and numericalsolutions on meshes S1, S2, and S3 of problem 3.1.

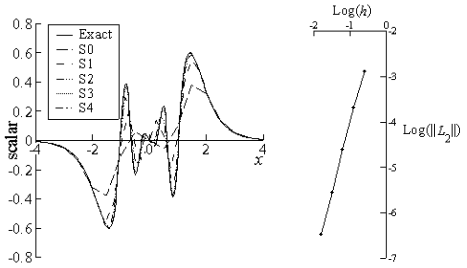

(a) (b)

Figure 4 (a) Comparison of exact and numerical solutions along y=0 and (b) Plot of L_2-norm errors of problem 3.1.

Table 1. L_2-norm errors and EOC of problem 3.1

Cell size	L_2 **-norm errors**
8/32	1.2952×10^{-3}
8/64	2.0803×10^{-4}
8/128	2.4924×10^{-5}
8/256	2.9171×10^{-6}
8/512	3.5045×10^{-7}
EOC	**1.97**

3.2 Rotation of Gaussian pulses

The Gaussian pulse scalar field is rotated around the domain $\Omega = [-0.5, 0.5]^2$. The initial condition [32]:

$$\phi_0(\boldsymbol{x}) = e^{-\frac{(x-x_{c_i})^2+(y-y_{c_i})^2}{2\sigma^2}} \qquad (25)$$

where $\boldsymbol{x}_c$ and σ are the center coordinates and the standard deviation, given by -0.25, 0, and 0.0447, respectively. The rotating velocity field with the angular velocity of 4 rad/s is imposed as $u(\boldsymbol{x}) = -4y$ and $v(\boldsymbol{x}) = 4x$. The end time is equal to $\pi/2$, which is the time period required for one turn rotation. The first test is a pure-convection case and the exact solution at $t=\pi/2$ is equal to the initial condition given by equation (25) above. The contour and the 3D carpet plots are presented in Figure 5(a). Figures 5(b)-(d) show the numerical solutions from the three uniform meshes S1, S2, and S3, respectively. The L_2-norm errors, minimum values, maximum values, and computational times obtained from various mesh sizes (S1 to S5) are presented in Table 2. The comparison of exact and numerical solutions, and a plot of the L_2-norm errors versus mesh sizes are shown in Figures 6(a) and 6(b), respectively. These figures highlight that the proposed method can provide a solution that converges to the exact solution as the mesh is refined with the EOC value of about two. Figure (6a) also shows that the undershooting of the numerical solutions diminishes on the refined meshes S3 and S4.

This problem is repeated again but with a diffusion coefficient of $\varepsilon = 10^{-4}$. The exact solution of such convection-dominated diffusion problem at $t=\pi/2$ is shown in equation (26) below. Its contour and the 3D carpet plots are shown in figure 7(a).

$$\phi_0(\boldsymbol{x}) = \frac{2\sigma^2}{2\sigma^2 + 4t\varepsilon} e^{-\frac{(x-x_{c_i})^2+(y-y_{c_i})^2}{2\sigma^2+4t\varepsilon}} \qquad (26)$$

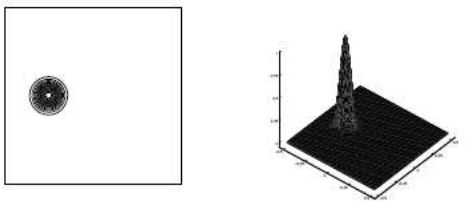

(a) Exact solution

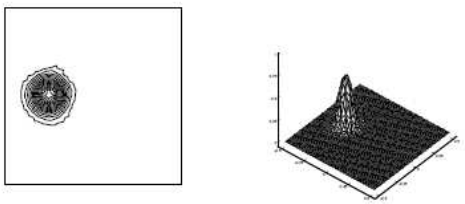

(b) S1

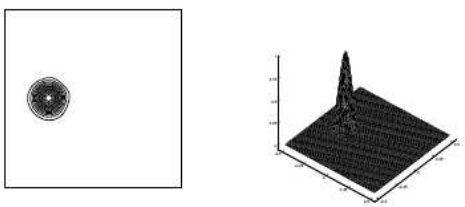

(c) S2

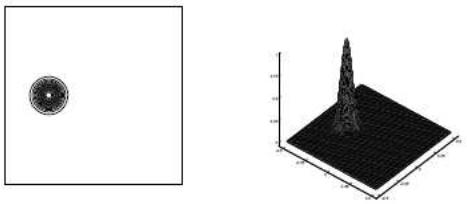

(d) S3

Figure 5 Comparison of exact and numerical solutions at time $t=\pi/2$ on S1, S2, and S3 of problem 3.2 ($\varepsilon = 0$).

Figures 7 (b)-(d) show the numerical solutions obtained from the three uniform meshes S1, S2, and S3, respectively. Again, the L_2-norm errors, minimum values, maximum values, and computational times obtained from various mesh sizes (S1 to S5) are presented in Table 3. The comparison of exact and numerical solutions, and the L_2-norm errors versus mesh sizes are shown in Figures 8(a) and 8(b), respectively. These figures again show that the proposed method can provide a solution that converges to the exact solution as the mesh is refined, with the EOC value of about two.

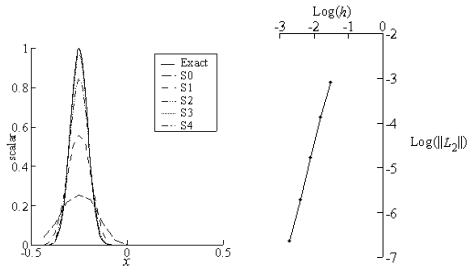

(a) (b)

Figure 6 (a) Comparison of exact and numerical solutions along y=0 and (b) Plot of L_2-norm errors of problem 3.2 ($\varepsilon = 0$).

Table 2 L_2-norm errors and EOC of problem 3.2 ($\varepsilon = 0$).

Cell size	L_2 **-norm errors**
1/32	8.0860×10^{-4}
1/64	1.3572×10^{-4}
1/128	1.6890×10^{-5}
1/256	1.9837×10^{-6}
1/512	2.3802×10^{-7}
EOC	**1.94**

Table 3. L_2-norm errors and EOC of problem 3.2 ($\varepsilon = 10^{-4}$).

Cell size	L_2 **-norm errors**
1/32	6.4558×10^{-4}
1/64	1.0063×10^{-4}
1/128	1.1653×10^{-5}
1/256	1.2259×10^{-6}
1/512	1.1471×10^{-7}
EOC	**2.12**

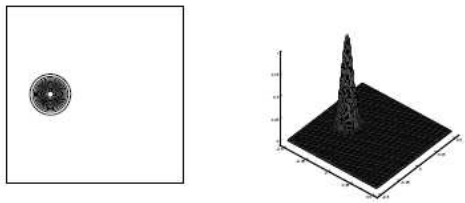

(a) Exact solution

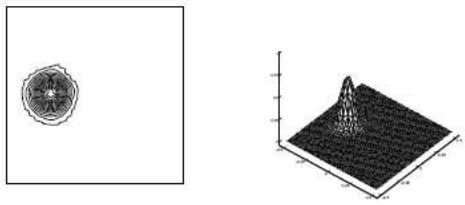

(b) S1

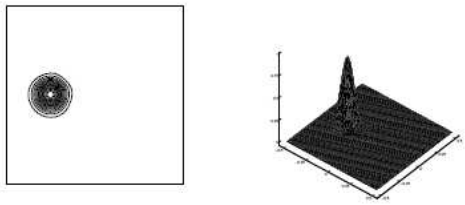

(c) S2

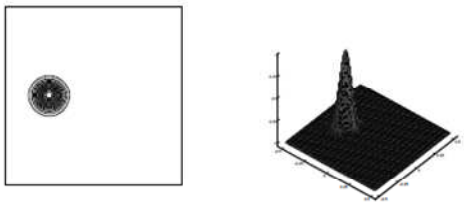

(d) S3

Figure 7 Comparison of exact and numerical solutions at time $t=\pi/2$ on S1, S2, and S3 of problem 3.2 ($\varepsilon = 10^{-4}$).

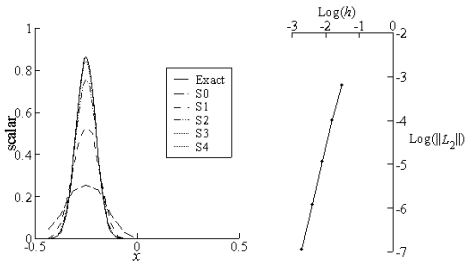

(a) (b)

Figure 8 (a) Comparison of exact and numerical solutions along y=0 and (b) Plot of L_2-norm errors of problem 3.2 ($\varepsilon = 10^{-4}$).

3.3 Half-Sine inflow Convection-Diffusion

The last example is the half-sine inflow convection-diffusion problem [4] on the domain $\Omega = [0,1]^2$. The initial condition is set to be zero and the boundary conditions at x=0 and x=1 are given by:

$$\phi_0(\boldsymbol{x}, t \geq 0) = \sin(\pi y) \quad (x = 0 \cap y \geq 0) \quad (27)$$

$$\phi_0(\boldsymbol{x}, t \geq 0) = 0 \quad (x = 1 \cap y \geq 0) \quad (28)$$

where the steady velocity field is given by $u(\boldsymbol{x}) = 1$ and $v(\boldsymbol{x}) = 0$. The diffusion coefficient, ε, for this convection-dominated diffusion a problem is equal to 0.0001. With such a small value of ε, the half sine inflow profile flows across the domain with small height drop until it approaches the outflow. The profile then drops suddenly to zero at the outflow boundary according to the condition on the right side of the domain. To reduce the oscillation at the outflow boundary, the Barth and Jespersen limiter function [28] is imposed.

The first test case of this problem is performed on a 16 × 16 grid size, and the numerical solutions at the four final times, t=0.25, 0.50, 0.75, and 2.0, are shown in Figures 9(a)-(d), respectively. There is a small height drop as described above and no oscillation appears in the solution. However, there is a slight overshoot along the front of the profile as the scalar quantity flows across the domain, because the mesh size is not small enough. This problem is examined again on a finer 32 × 32 grid, and the numerical solution at the same four time steps are presented in Figures 10(a)-(d). These figures show that as the grid size becomes smaller, the overshoot of the front profile disappears. With this mesh, the proposed method does not produce any numerical oscillation, while the artificial diffusion is not added into the solution. The computed solution thus does not suffer from excessive diffusion as it marches out in time. To assess the behavior of the scheme when applied to steady-state problems, this problem is performed again on both meshes until the final time reaches t=8. The convergence histories of the scheme on both meshes are shown in Figure 11 by plotting L_2-norm of scalar residual versus time. The figure indicates that the steady-state solution is reached at a time of about two.

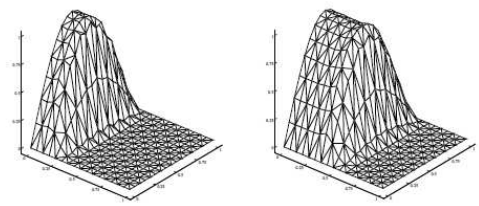

(a) t=0.25 (b) t=0.5

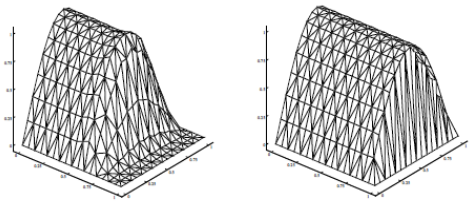

(c) t=0.75 (d) t=2.0

Figure 9 Numerical solutions on 16 × 16 grid size at four different times of problem 3.3.

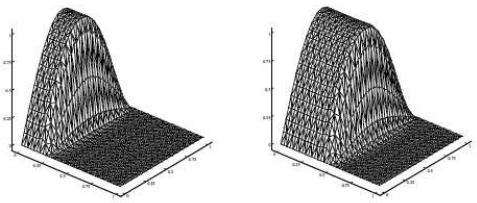

(a) t=0.25 (b) t=0.5

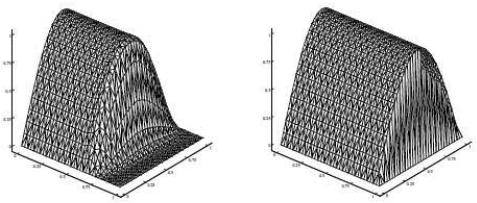

(c) t=0.75 (d) t=2.0

Figure 10 Numerical solutions on 32 × 32 grid size at four different times of problem 3.3.

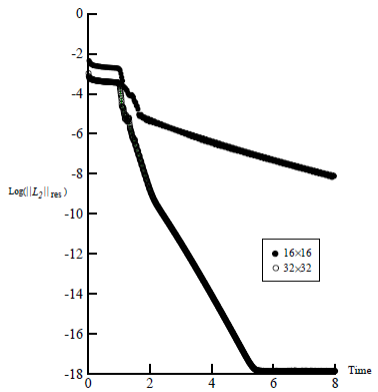

Figure 11 Convergence histories for solutions on 16 × 16 and 32 × 32 grid sizes of problem 3.3.

4. Conclusion

An explicit finite volume element method for solving the two-dimensional convection-diffusion equation on triangular meshes is presented. The theoretical formulation of the method is explained in details. The method employs the weighted residuals concept in the finite element technique for estimating the gradient quantities at the cell faces. Three numerical examples are used to evaluate the robustness and accuracy of the proposed method. These examples show that the method provides accurate solutions without requiring artificial diffusion. The solution behavior and its accuracy are improved as the mesh is refined.

5. Acknowledgement

The authors are pleased to acknowledge the Thailand Research Fund (TRF) for supporting this research work.

6. References

[1] Brooks A. N. and Hughes T. J. R., Streamline Upwind Petrov-Galerkin Formulation for Convection Dominated Flows with Particular Emphasis on the Incompressible Navier-Stokes Equation, Comput. Methods Appl. Mech. Engrg., Vol. 32, pp. 199-259, 1982.

[2] Codina R., Comparison of Some Finite Element Methods for Solving the Diffusion-Convection-Reaction Equation, Int. J. Numer. Meth. Engrg., Vol. 156, pp. 185-210, 1998.

[3] Kohler T. and Voss D., Second-Order Methods for Diffusion-Convection Equations, Commun. Numer. Meth. Engng., Vol. 15, pp. 689-699, 1999.

[4] Heitmann N. and Peurifoy S., Stabilization of the Evolutionary Convection-Diffusion Problem: Introduction and Experiments, Proceed-

ings of the SSHE-MA Spring 2007 Conference, 2007.

[5] Toro E. F., Riemann Solvers and Numerical Methods for Fluid Dynamics, 2nd Edition, Springer-Verlag, Berlin, 1999.

[6] Godunov S. K., A Difference Scheme for Numerical Computation of Discontinuous Solution of Hydrodynamic Equations, Math. Sb., Vol. 47, pp. 271-306, 1959.

[7] Harten A., High Resolution Schemes for Hyperbolic Conservation Laws, J. Comput. Phys., Vol. 49, pp. 357-393, 1983.

[8] Shu C. W., TVB Uniformly High-Order Schemes for Conservation Laws, Math. Comp., Vol. 49, pp. 105-121, 1987.

[9] Boris J. P. and Book, D. L., Flux-Corrected Transport I. SHATA, A Fluid Transport Algorithm that Works, J. Comput. Phys., Vol. 11, pp. 38-69, 1973.

[10] Leonard B. P., Simple High-Accurate Resolution Program for Convection Modeling of Discontinuities, Int. J. Num. Meth. Fluids, Vol. 8, pp. 1291-1318, 1988.

[11] Tamamidis P. A., New Upwind Scheme on Triangular Meshes using the Finite Volume Method, Comput. Methods Appl. Mech. Engrg., Vol. 124, pp. 15-31, 1995.

[12] Batten P., Lambert C. and Causon D. M., Positively Conservative High-Resolution Convection Schemes for Unstructured Elements, Int. J. Numer. Meth. Engrg., Vol. 39, pp. 1821-1838, 1996.

[13] Kurganov A. and Tadmor E., New High-Resolution Central Schemes for nonlinear Conservation Laws and Convection-Diffusion Equations, J. Comput. Phys., Vol. 160, pp. 241-282, 2000.

[14] Juntasaro V. and Marquis A. J., Comparative Study of Flux-Limiters based on MUST Differencing Scheme, Int. J. CFD, Vol. 18, pp. 569-576, 2004.

[15] Man C. and Tsai C. W., A Higher-Order Predictor-Corrector Scheme for Two-Dimensional Advection-Diffusion Equation, Int. J. Num. Meth. Fluids, Vol. 56, pp. 401-418, 2007.

[16] Waterson N. P. and Deconinck H., Design Principles for Bounded Higher-Order Convection Schemes-A Unified Approach, J. Comput. Phys., Vol. 224, pp. 182-207, 2007.

[17] Ni R. H., Multiple Grid Scheme for Solving the Euler Equations, AIAA paper 81-1025, 1981.

[18] Rossow C. C., Accurate Solution of the 2D Euler Equations with an Efficient Cell-Vertex Upwind Scheme, AIAA paper 93-0071, 1993.

[19] Hall M., A Vertex-Centroid Scheme for Improved Finite-Volume Solution of the Navier-Stokes Equations, AIAA pp. 91-1540, 1991.

[20] Barth T. J. and Ohlberger M., Finite Volume Methods: Foundation and Analysis, chapter in Encyclopedia of Computational Mechanics, edited by Stein, E., de Borst, R. and Hughes, T.J.R., John Wiley & Sons, Chichester, 2004.

[21] Jameson A., Schmidt W. and Turkel E., Numerical Solutions of the Euler Equations by Finite Volume Methods using Runge-Kutta Time-Stepping Schemes, AIAA paper 81-1259, 1981.

[22] Frink N. T., Upwind Scheme for Solving the Euler Equations on Unstructured Tetrahedral Meshes, AIAA J., Vol. 30, pp. 70-77, 1992.

[23] LeVeque R. J., High-Resolution Conservative Algorithms for Advection in Incompressible Flow, SIAM J. Numer. Anal., Vol. 33, pp. 627-665, 1996.

[24] Harten A., On a Class High Resolution Total-Variation-Stable Finite-Difference schemes, SIAM J. Numer. Anal., Vol. 21, pp. 1-23, 1984.

[25] Ben-Artzi M. and Falcovitz J., A Second-order Godunov-type Scheme for Compressible Fluid Dynamics, J. Comput. Phys., Vol. 55, pp. 1-32, 1984.

[26] Ben-Artzi M., Application for the Generalized Riemann Problem Method of 1-D Compressible Flows with Material Interfaces, J. Comput. Phys., Vol. 65, pp. 170-178, 1986.

[27] Guinot V., An Unconditionally Stable, Explicit Godunov Scheme for Systems of Conservation Laws, Int. J. Numer. Meth. Fluids, Vol. 38, pp. 567-588, 2002.

[28] Barth T. J. and Jespersen D. C., The Design and Application of Upwind Schemes on Unstructured Meshes, AIAA paper 89-0366, 1989.

[29] Zienkiewicz O. C., Nithiarasu P., Codina R., Vezquez M. and Ortiz P., The Characteristic-Based-Split Procedure: An Efficient and Accurate Algorithm for Fluid Problems, Int. J. Num. Meth. Fluids, Vol. 31, pp. 359-392, 1999.

[30] Billett S. J. and Toro E. F., On WAF-type Schemes for Multidimensional Hyperbolic Conservation Laws, J. Comput. Phys., Vol. 130, pp. 1-24, 1997.

[31] Zienkiewicz O. C. and Taylor R. L., The Finite Element Method for Solid and Structural Mechanics, 6th Edition Elsevier Butterworth-Heinemann, Burlington, 2005.

[32] Wang H., Gahle H. K., Ewing R. E., Espedal M. S., Sharpley R. C. and Man S., An ELLAM Scheme for Advection-Diffusion Equations in Two Dimensions, SIAM J. Sci. Comput., Vol. 20, pp. 2160-2194, 1999.